stellarator news

**Published by Fusion Energy Division, Oak Ridge National Laboratory**
**Building 9201-2 P.O. Box 2009 Oak Ridge, TN 37831-8071, USA**

Editor: James A. Rome Issue 43 January 1996
E-Mail: jar@ornl.gov Phone: (423) 574-1306 Fax: (423) 576-7926

## H-1 Heliac to be upgraded to a national facility

On the 6th of December 1995, the Australian Prime Minister, Paul Keating, announced a grant of AU$8.7M to upgrade the H-1 Heliac at the Australian National University (ANU) in Canberra to a "major national research facility" to be called H-1NF.

This announcement was part of a AU$428M science innovation package "Innovate Australia" which is described in more detail on the following World Wide Web page:

http://www.das.gov.au/~dist/events/innovate/r1.html

"Innovate Australia" includes the funding of seven facilities for a total of AU$62M, and is the result of the first formal round of applications for national research facility funding, for which more than 60 expressions of interest were received. Previously, national facilities in Australia were funded on a case-by-case basis when the need or opportunity arose. Plasma physicists were delighted by the recognition of their work and by the opportunity to take their research to the leading edge of advanced magnetic confinement systems. Science policy commentators were encouraged that the government considered the science innovation statement to be of sufficient importance that the Prime Minister should be directly involved, along with the Science Minister, Senator Peter Cook.

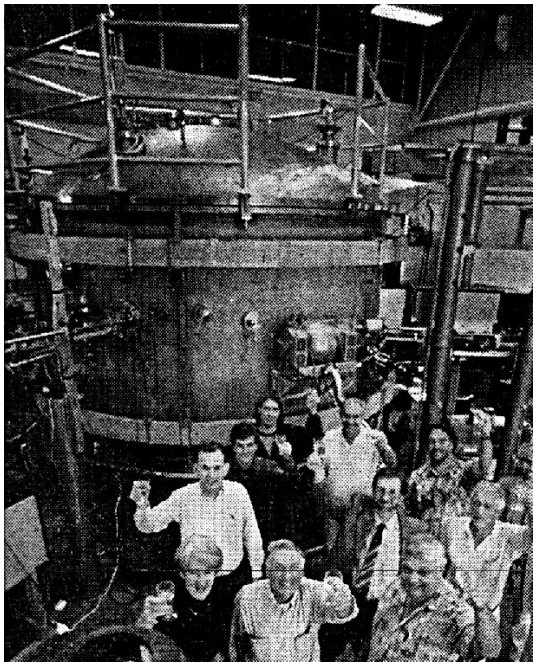

The H-1 Team celebrating the grant that was received from the Australian government to upgrade the machine.

The major national research facility grant will turn the H-1 Heliac fusion plasma physics experiment at the Australian National University into a fusion research facility of truly international importance for scientists in the Australian Fusion Research Group (AFRG) and from overseas. The AFRG is a consortium of scientists currently working in research associated with high-temperature plasma physics in six universities (University of Canberra, University of New England, Central

## *In this issue . . .*

Queensland University, Flinders University, University of Sydney, and Research School of Physical Sciences and Engineering at the ANU). The consortium is associated with the Australian Institute of Nuclear Science and Engineering (AINSE). The AFRG recognizes that a fusion experiment of international standing, such as an upgraded H-1 Heliac facility, would be the focus of innovative plasma physics research in a wide range of areas, in addition to fusion-oriented plasma physics, such as spectroscopy, laser and optical diagnostics, real-time data processing, nonlinear dynamics, and computational physics.

International collaboration will be an important aspect of the operation as a national facility and is facilitated by the *IEA Implementing Agreement on Stellarator Research*. Collaboration under an ANU-NIFS (National Institute of Fusion Science, Japan) agreement is well under way after visits in both directions in late 1995.

In the national facility upgrade, electron and ion heating systems will be added; the laboratory and some of the other systems will be upgraded to improve performance so as to reach more fusion-relevant plasma conditions. The upgrade, using the original coil set, will also increase the machine availability and reliability to accommodate collaborating groups efficiently. The budget for the purchase and installation of the following equipment was proposed to be spread over three years, starting as soon as practicable. The three largest items, two heating systems and the magnet supply and line, each account for about 25% of the budget.

The primary enhancements will be

- 1-MW electron cyclotron heating (ECH) gyrotron source for heating plasma to highest temperatures (~1 keV) and lowest collisionality.
- 1-MW radiofrequency source for obtaining highest plasma pressure beta > 2% and allowing nonresonant heating for magnetic field scans.
- A new primary power line, switching, and a transformer will feed 10-MW magnet power supplies to allow reliable operation at high magnetic fields at a reasonable repetition rate (1 minute), unlimited by the magnetic configuration or by external factors such as grid load.

Also included are vacuum system enhancements and cryopump, lasers, and millimeter wave sources for plasma diagnostics and modifications to the machine hall. The data system will be enhanced, and the network interface upgraded to allow collaboration (remote analysis and some remote control) directly from remote sites around Australia and, to a limited extent, from overseas.

Boyd Blackwell for the H-1 group and the AFRG
E-Mail: bdb112@rsphy3.anu.edu.au

## LID experiments in CHS

A series of local island divertor (LID) experiments has just started that intends to demonstrate the principle of the LID on the Compact Helical System (CHS) in Nagoya, Japan.

Control of the edge plasma is one of the key research issues for the Large Helical Device (LHD), which is a superconducting heliotron-type device under construction at the National Institute for Fusion Studies (NIFS) in Toki, Japan. We plan to use the LID on LHD, prior to installing a closed full helical divertor.

The LID is a divertor that uses an $m/n = 1/1$ island, formed in the edge region. The advantage of the LID over the closed full helical divertor is the technical ease of hydrogen pumping because the hydrogen recycling is toroidally localized. However, the LID functions have not been studied and verified experimentally.

For the CHS experiment, 16 small perturbation coils are used to form an $m/n = 1/1$ island. When a resonant perturbation field generated by two pairs of perturbation coils located just above and below the CHS vessel is added to the standard CHS magnetic configuration, an $m/n = 1/1$ island appears at the $\iota = 1$ surface, together with $m/n = 2/1$ islands, which appear because of the toroidal coupling at the $\iota = 0.5$ surface. The $m/n = 2/1$ islands, however, can be almost completely eliminated by a proper arrangement of the perturbation coil currents. The outward heat and particle fluxes crossing the island separatrix flow along the field lines to the back side of the island, where carbon target plates 10 mm thick, are placed on a divertor head. The particles recycled there are pumped out by a cryogenic pump with pumping speed of 21,000 L/s.

The geometrical shapes of the divertor head and pumping duct are designed to form a closed divertor configuration with high pumping efficiency. Unlike conventional pump limiters, the leading edges of the divertor head (which consists of carbon target plates) are situated inside the island, thereby being protected from the high outward heat flux from the core.

Formation of an $m/n = 1/1$ island was demonstrated experimentally by a mapping technique of the magnetic surface. We adopted the fluorescent method, which uses an electron gun with a tungsten filament and a fluorescent mesh that emits light when the electrons strike the mesh. From the distribution of the electron striking points on the mesh, observed by a CCD TV camera, the geometry of the flux surface was identified. By varying the radial position of the electron gun, we obtained the information on the whole flux surface structure including an $m/n = 1/1$ island whose

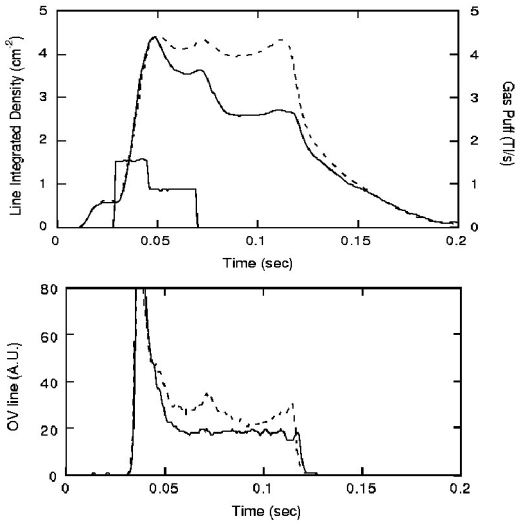


**Fig. 1.** Comparisons of line-integrated electron density and OV radiation intensity between discharges with (solid line) and without (dotted line) the perturbation field. The time sequence of gas puffing is also shown in the figure.

maximum width is about 4 cm. The observed island structure is consistent with the theoretical prediction.

CHS was operated with a toroidal magnetic field of 0.9 T and a magnetic axis position $R_{ax}$ = 99.5 cm. When $R_{ax}$ > 97.4 cm, the $\iota$ = 1 flux surface is well inside the vacuum vessel wall. The plasma was initially produced by ion cyclotron resonant frequency (ICRF) or by second harmonic electron cyclotron resonant heating (ECRH) and heated by the tangential neutral bean injection (NBI) with 0.82 MW at 38 keV. The temperature profile on the carbon plates was measured by an infra-red TV camera and shows that the position of the maximum temperature rise changes as the position of the divertor head is changed and that it is situated about 1 cm away from the leading edge when the leading edge is well inside the island. This finding suggests that there is no leading-edge problem, as expected. The maximum temperature rise on the carbon plates during the discharge was observed to be about 5°C. With the divertor head in a right position and the perturbation field on, the neutral particle pressure in the plenum, measured by an ASDEX style fast-ion gauge, becomes a factor of 1.5–2 higher than in the case without the perturbation field. The LID experiment has been done under a collaboration with Oak Ridge National Laboratory (ORNL) from its beginning. ORNL staff have made significant contributions to the neutral pressure measurement using the fast-ion gauge.

The $H_\alpha$ radiation intensity behind the divertor head, monitored by a CCD TV camera with an optical filter, behaves similarly to the neutral pressure. Furthermore, the Langmuir probe measurement showed that the ion saturation current measured behind the divertor head becomes higher by a factor of 1.5–2 with the perturbation field on, than without the perturbation field. These results clearly demonstrate that the particle flow is indeed guided to the back side of the divertor head by the island magnetic field structure, the fundamental function of this type of divertor.

The plasma parameters are found to change when the island is formed. With the perturbation field on and at a fixed level of gas puffing, the line-average electron density and the OV radiation intensity decrease, compared with those without the perturbation field, as shown in Fig. 1. The stored energy measured with a diamagnetic loop is kept almost constant under this condition, which is accompanied by an increase in the electron temperature measured by the YAG Thomson scattering system. A comparison of the stored energy was made between the discharges with and without the perturbation field at fixed line-average density. We found that the stored energies in the discharges with the perturbation field are about 20% higher than those without the perturbation field, indicating a modest improvement of the energy confinement.

The experimental data described here are still preliminary, and further experimental study is needed. But the results so far are encouraging in terms of the effectiveness of the LID. The LID experiment will be continued until the end of March 1996.

To close, we would like to describe the status of the LID construction for the LHD. The National Diet passed the bill for the second supplementary budget at the end of October 1995, and a capital budget was approved to construct the LID system for the LHD. In this fiscal year, we will fabricate 20 copper coils that generate resonant perturbation fields and 3 electric power supplies that provide the electric currents into the coils. The coils will be installed around all upper and lower ports of the LHD cryostat to generate a maximum magnetic field of about 30 gauss on the equatorial plane. With these coils, an island with a full width of about 15 cm can be maintained in a steady-state discharge with a toroidal magnetic field of 3 T. The three electric power supplies are designed to eliminate other unnecessary islands (which are usually formed by toroidal coupling) by a proper arrangement of coil currents. For pulsed operations, a factor of 1.4 wider island can be created. This system can also be used to eliminate the natural islands, which may be produced by error fields, for example, due to a small misalignment of the helical or poloidal coils and ferromagnetic material located near the LHD.

A. Komori and the LID Team National Institute for Fusion Science
Nagoya 464-01, Japan
Phone: +81-572-57-5603
FAX: +81-572-57-5600
E-mail: komori@nifs.ac.jp

# Ion heat transport in W7-AS in the lmfp regime

In the W7-AS experiment, access to the ion long mean free path (lmfp) regime turned out to be a serious problem even at high heating power. Central ion temperatures were restricted to about 1 keV [1]. Electrons can be raised to temperatures up to 3 keV using electron cyclotron resonant heating (ECRH). ECRH thus provides access to the deep lmfp regime for the electrons. However, to achieve the lmfp regime for ions, neutral beam injection (NBI) heating has to be used to provide direct ion heating in order to obtain the necessary high ion temperatures. Unfortunately, discharges with high-power NBI heating lead to high densities, and so the temperatures generally stay low. Substantial additional ECRH power was mandatory to obtain density control and stationary conditions in this case [2]. This result can be explained by a particle diffusivity $D$, which scales roughly as $D \propto P/n$ at the plasma edge.

Recently, access to the ion lmfp regime was obtained using substantial NBI heating at fairly low additional ECRH power with stationary conditions at densities of about $5 \times 10^{13}$ cm$^{-3}$. Very good wall conditions are essential to ensure recycling control under these conditions. At still lower densities, the NB heating efficiency degrades.

### Neoclassical transport

In the following, we discuss the barrier to obtaining high ion temperatures within the framework of neoclassical theory. For the flat or even slightly hollow density profiles characteristic of stellarators, rather small radial electric fields $E_r$ are expected. Only in the density gradient region are significant values $E_r < 0$ predicted. These neoclassical predictions based on the ambipolarity condition of the particle fluxes are reasonably well confirmed by active charge-exchange recombination spectroscopy (CXRS) measurements [3]. Starting from the plateau collisionality regime, where the ion heat flux scales as $Q_i \propto T_i^{5/2}$, the adjacent $1/\nu$ regime with the scaling $Q_i \propto T_i^{9/2}$ at very small $E_r$ represents the barrier to obtaining higher ion temperatures and thus lower collisionalities, $\nu^* = \nu R/\iota v_{th} \propto n/T^2$, at fixed density (see the right part of Fig. 1). With increasing negative $E_r$, access to the so-called $\sqrt{\nu}$ regime with $Q_i \propto T_i^{3/2}$ is obtained [4]. The "tokamak-like" $\nu$ regime with $Q_i \propto T_i^{1/2}$ applies for very low $\nu^*$ only (left part of Fig. 1). In the intermediate lmfp regime, where the neoclassical electron heat transport coefficients are less than the ion ones, the feature of the "electron root" [5] with rather strong $E_r > 0$, for which the neoclassical electron transport coefficients are significantly decreased, does not appear, and the electrons stay in the $1/\nu$ regime.

Neoclassical transport estimates for the complex 3D magnetic field topology of W7-AS are based on a

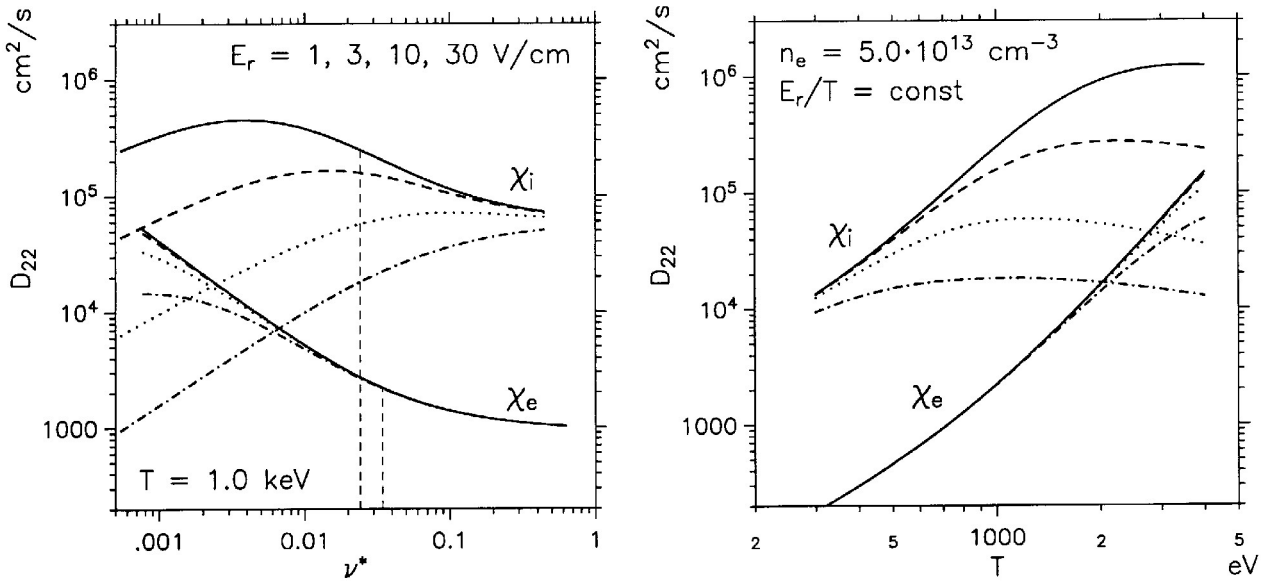


**Fig. 1.** Neoclassical electron and ion heat diffusivities (diagonal term in the transport matrix) for an improved W7-AS configuration ($r$ = 10 cm, $B_0 \approx 2.5$ T, $B_z$ = 200 G) with the radial electric field as parameter. On the left: versus the collisionality $\nu^*$ for fixed temperature (1 keV) and with $E_r$ = 1 V/cm (solid lines), 3 V/cm (dashed lines), 10 V/cm (dotted lines), and 30 V/cm (dot-dashed lines). $\nu^*$ for typical parameters ($T_e = T_i$ = 1 keV, $n_e \approx 5 \times 10^{13}$ cm$^{-3}$) is marked by dashed vertical lines. On the right: $\chi_i, \chi_e$ versus temperature for fixed density (i.e., $\nu^*$ increases to the left) and $E_r \propto T$ (the values given in the left figure apply for $T$ = 1 keV).

database of DKES calculations. The DKES code [6] solves the monoenergetic drift-kinetic equation for general Fourier spectra of $B$ on each flux surface, depending on the collisionality and radial electric field. To reduce the amount of DKES computations, numerical fits of the mono-energetic diffusion coefficients to the DKES results in the different collisionality regimes, where the functional dependence of these coefficients is equivalent to those of traditional analytic theory, have been developed [4]. This technique leads to a very good representation of the neo-classical transport properties for the different W7-AS configurations and is rather efficient for the energy convolution to calculate the thermal $2 \times 2$ transport matrix.

For low $\iota \approx 1/3$, where the higher harmonics in the $B$-Fourier spectrum are less pronounced than for $\iota \approx 1/2$, two different concepts for neoclassically improved configurations have been analyzed [7]: (1) the inward shift of the plasma column by applying a vertical field similar to that in torsatrons and (2) the application of a local increase of the magnetic field strength in the region of strong toroidal curvature (elliptical plasma cross-section), shifting a significant portion of the ripple-trapped particles to the straighter part of the magnetic axis (with the triangular plasma cross-section). For both optimized configurations a transport improvement by a factor of about 2 was found in the $1/\nu$ regime with respect to the standard configuration in the DKES calculations. This improvement holds also for small $E_r$ in the $\sqrt{\nu}$ regime [4].

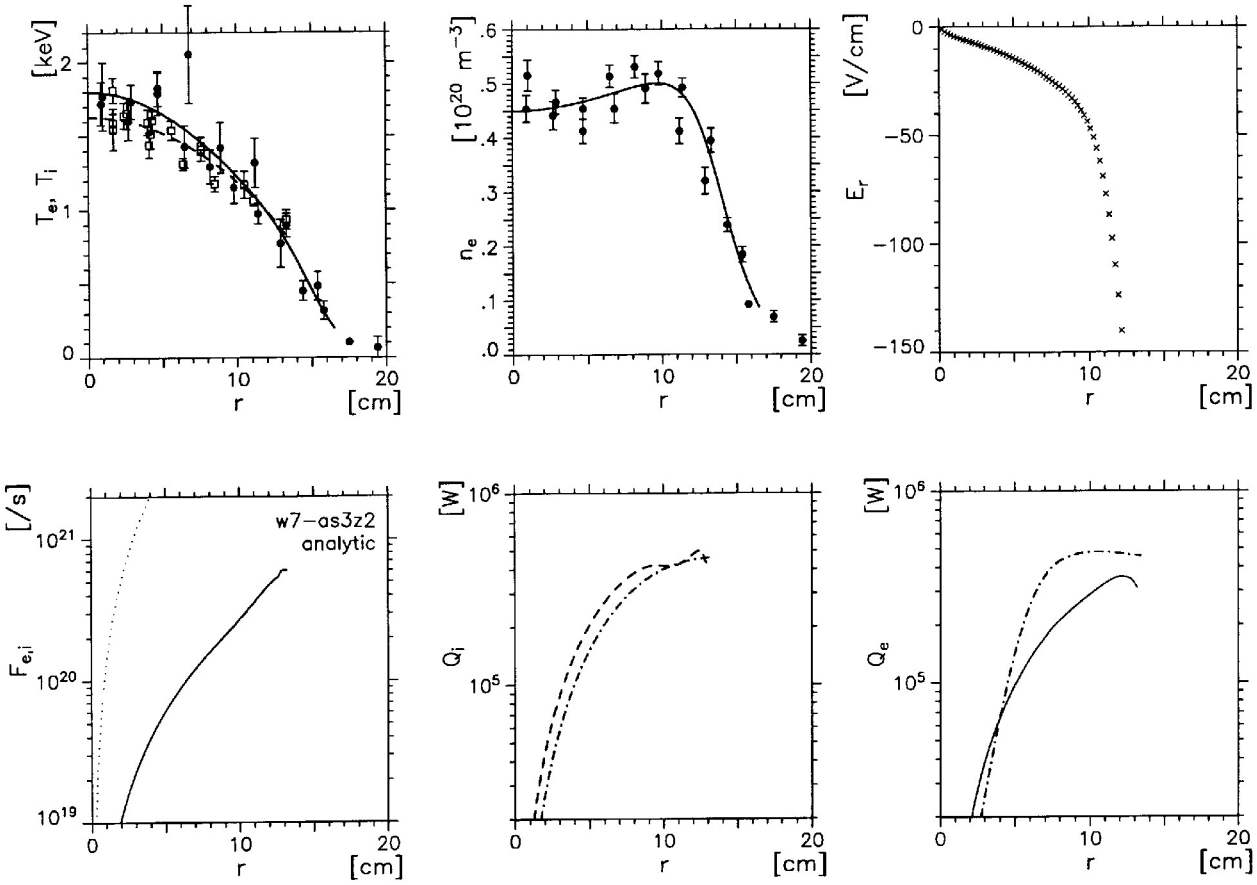


**Fig. 2.** Profiles, transport analysis, and neoclassical predictions for a stationary discharge with combined ECRH and NB heating ($B_0$ = 2.5 T, $B_z$ = 260 G).
Upper row: electron (solid line, full dots from Thomson) and ion temperatures (dashed line, open squares from CX) on the left; electron density (from Thomson) in the center; and the calculated ambipolar radial electric field $E_r$ on the right.
Lower row: ambipolar neoclassical particle flux on the left; ion heat flux $Q_i$ (neoclassical prediction: dashed line, from power balance: dot-dashed line) in the center; and electron heat flux $Q_e$ (neoclassical prediction: solid line, from power balance: dot-dashed line) on the right.

### Combined ECRH and NB heating experiments

In the last experimental campaign, rather high vertical fields ($B_z \approx 200$–$260$ G at 2.5 T) had to be used to control the plasma radius because of the removed upper and lower rail limiters. This situation resulted in one of the above mentioned transport-reduced magnetic field configurations [1], where with $T_i(0)$ up to 1.6 keV at $n_e(0) \approx 5 \times 10^{13}$ cm$^{-3}$, the highest ion temperatures have been obtained so far.

In Fig. 2, measured profiles for such a discharge are shown together with the results of the transport analysis and the neoclassical predictions. The discharge was heated by 400-kW ECRH and by three NB sources with co-injection. The powers absorbed by electrons and ions are about 650 kW and 600 kW, respectively. The FAFNER code Monte Carlo calculations indicate a fairly peaked ion heating profile with about 2/3 of the NB power being absorbed by the ions bacause of the rather high electron temperatures ($T_e(0) \approx 1.8$ keV). With counter-injection, the global NB heating efficiency is reduced, and a flat ion heating profile is predicted. Ion temperature data from the active CX diagnostic are available for $r \leq 13$ cm only, and so the transport analysis (Fig. 2) is restricted to this range. The ion heat flux $Q_i^{neo}$ only slightly exceeds the experimental value from the power balance. For these experiments with H injection into a $D^+$ target plasma, a rather high ratio of $H^+$ to $D^+$ (roughly 1:1) is indicated. The $Q_i^{neo}$ given is estimated on the assumption of pure $H^+$, and $Q_i^{neo}$ turned out to be about 20% higher for $D^+$. Some additional uncertainty is introduced in the neoclassical prediction because DKES results for $B_z = 200$ G are used instead of the 260 G in the experiments; furthermore, the monoenergetic transport coefficients in the $\sqrt{\nu}$ regime are scaled by an improvement factor of 2 (see the first section) with respect to the standard configuration ($B_z = 0$). With these restrictions, fairly good agreement of the neoclassical ion heat flux, where $E_r$ from the ambipolarity condition is included, with the experimental power balance is found. The electron heat flux estimated from the power balance exceeds the neoclassical prediction by a factor of up to 2. However, some uncertainty is introduced by the smoothed $T_e$ profile, which is used for the neoclassical predictions, in the region of the ECRH power deposition expected slightly off axis at about 4 cm because of the Shafranov shift.

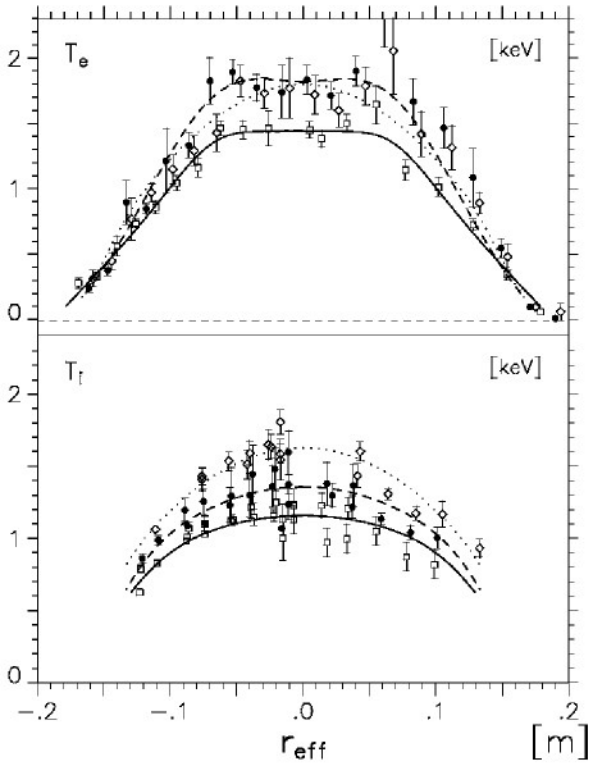


**Fig. 3.** Electron (from Thomson scattering, upper plot) and ion (from CX diagnostic, lower plot) temperature profiles for a NB heating power scan ($B_0 = 2.5$ T, $B_z = 260$ G). Solid lines: 400 kW ECRH and 1 NB source; dashed lines: 700 kW ECRH and 2 NB sources; dotted lines: 400 kW ECRH and 3 NB sources (same discharge as in Fig.2).

The neoclassical particle flux, $\Gamma_i^{neo} = \Gamma_e^{neo}$, is roughly consistent with the beam fueling rate in the region of the flat density profile, $r \leq 10$ cm. In this inner region, fairly small $E_r$ values of up to 40 V/cm are predicted (Fig. 2), and the ambipolar particle flux is mainly driven by the off-diagonal term ($\propto \nabla T$) in the transport matrix. Nevertheless, these electric fields are sufficient to reduce the neoclassical ion heat transport by more than an order of magnitude (see Fig. 1). They allow access to the $\sqrt{\nu}$ regime and thus to high $T_i$ values. The strong density gradient at $r \geq 11$ cm drives the $E_r$ strongly negative. Here, the particle sources due to recycling become dominant (almost no external gas puffing was necessary to maintain the discharge).

Later in this discharge the ECRH was completely switched off. No fully stationary conditions could be obtained because the line-averaged density was slightly increasing. About 40 ms after ECRH switch-off, $T_i$ was nearly unchanged, whereas $T_e(0)$ was decreased by 500 eV ($T_i > T_e$). The transport analysis leads to similar conclusions; i.e., fairly good agreement of the neoclassical predictions with the power balance is found. In Fig. 3, the electron and ion temperatures are shown for an NB power scan with 1 to 3 co-sources (about 250 to 300 kW of heating power each), where the density profiles are similar to that of Fig. 2. The ion heating by the NB's is dominant, the collisional power transfer $P_{ei}$ being of minor importance. Even in the scenario with 700-kW ECRH and 2 NB sources, where the central $T_e$ significantly exceeds $T_i$, $P_{ei}$ in the region $r \leq 12$ cm is

well below 100 kW. The analysis of the ion heat flux from the power balance at $r$ = 10 cm (where the density gradients vanish) leads to a temperature dependence of about $Q_i \propto T_i^{3/2}$ in agreement with the $\sqrt{\nu}$ regime scaling. With all uncertainties taken into account, access to the lmfp regime with improved neoclassical confinement is directly confirmed.

First experiments with a slightly transport-enhanced magnetic configuration in W7-AS do not allow such clear conclusions. By increasing the current in the large special coils located in the region of strong toroidal curvature with respect to the other MF coils system by 30%, higher losses are indicated by the "bounce-averaging" of the $\nabla B$ drift on flux surfaces [7] than with the transport-reduced configurations of the first section. Indeed, both the electron and ion temperatures were reduced by about 15% in the experiments. However, the average magnetic field is also 7% smaller for this configuration, and the neoclassical transport coefficients scale as $B^{-2}$. As the DKES database and exact NB heating profiles for this configuration are not available at present, changes in the neoclassical heat flux due to the modified magnetic field configuration cannot be discriminated sufficiently well against changes due to $Q_i \propto T_i^{3/2}/B^2$.

**References**


[1] Kick M. et al., *Proc. 10th Int. Conf. on Stellarators, IAEA Techn. Committee Meeting*, Madrid, Spain, May 22–26, 1995.

[2] Ringler H. et al., *EPS 1990 Plasma Phys. Control. Fusion* **32**, 933.

[3] Baldzuhn J. et al., *Proc. 10th Int. Conf. on Stellarators, IAEA Techn. Committee Meeting*, Madrid, Spain, May 22–26, 1995.

[4] Beidler C. D. et al., 1994 Europhysics Conference Abstracts (*Proc. 21th EPS Conference on Controlled Fusion and Plasma Physics*), EPS, Montpellier, France, **18B** (Pt. II), 568 (1994).

[5] Maassberg H. et al., *Phys. Fluids*, **B5,** 3627 (1993).

[6] Hirshman S. P. et al., *Phys. Fluids*, **29,** 2951 (1986), van Rij W. I. and Hirshman S. P., *Phys.Fluids*, **B1,** 563 (1989).

[7] Beidler C. D., et al., *Proc. 10th Int. Conf. on Stellarators, IAEA Techn. Committee Meeting*, Madrid, Spain, May 22–26, 1995.



M. Kick and H. Maassberg for the W7-AS, ECRH, and NBI Teams
IPP Garching, EURATOM-Association,
Garching bei München, Germany
Phone: 0049-89-3299-2122
E-Mail: kick@ipp-garching.mpg.de


# Status of the Large Helical Device (LHD) project

## Status of LHD construction at Toki

575 out of 900 turns of the superconducting helical coil have been completed. The winding accuracy is quite good, namely within 2 mm. Winding of the lower outer vertical field coil has been completed, and winding of the upper coil has commenced. Recently, the LHD vacuum pumping system was ordered from industry, and delivery is expected next March.

## Progress of superconducting coil fabrication and research on cryogenics and applied superconductivity

### *Performance of the helical coil winding machine*

A computer-controlled helical coil winding machine has been developed for the LHD project that significantly reduces the technical difficulties of winding the helical coil. The winding machine primarily consists of conductor shaping and supply devices, ten up-down supports, a center stage, a working floor, and a set of numerical control units.

The conductor is bent and twisted by the shaping and supply devices. Driving axes for the winding machine are numerically controlled because the helical coils possess a complicated three-dimensional structure.

**Table 1.** Major Specifications of the winding machine

| | |
|---|---|
| Precision of shaping (%) | 10 |
| Plastic strain (%) (bending) | < 0.82 |
| (torsion) | < 0.69 |
| Length of a conductor (m) | < 1200 |
| Number of NC axes | 13 |
| Size of working room (m) | 22.0 m x 23.3 |
| Height of clean room (m) | 12.4 |
| Work weight (ton) | < 320 |
| Load on a up-down support (ton) | < 180 |

### *Mass production of helical coil conductors*

The helical coil conductor, a fully cryostable NbTi superconductor with aluminum stabilizer, has been developed to satisfy the requirements 13 kA at 7 T and 4.4°K. It is also possible to generate 4 T at 1.8°K in Phase II with superfluid helium.

The conductor consists of 15 NbTi superconducting strands, aluminum stabilizer covered with a cupro-nickel sheath, which are enclosed in a copper housing. The conductor surface is oxidized to enhance the heat transfer to liquid helium. A total of 38 conductors has been tested to ensure the performance of this conductor. These results show that the critical current is more than

1.7 times the operating current and that the recovery current is higher than the operating current.

### *Helical coil winding*

The helical coil is wound in a helical coil case made of thick stainless steel. The case is used as a bobbin as well as a liquid helium bath. The helical coils have 450 turns each, and the total length is 37 km. Ground insulation is pasted directly on the can and cured by autoclaving. The on-site winding of helical coils started at the beginning of 1995 and will be completed by the summer of 1996.

**Table 2.** Major parameters of the helical coil

| Item | Phase I | Phase II |
|---|---|---|
| Coil temperature (°K) | 4.4 | 1.8 |
| Current (kA) | 13 | 17.3 |
| Maximum field (T) | 6.9 | 9.2 |
| Magnetic stored energy (GJ) | 0.92 | 1.64 |
| Number of turns | 450 (150 × 3) | |
| Spacer factor (%) | 30–70 | |
| Spacer pitch (mm) | 49.2–64.3 | |
| Positioning error (mm) | < 2 | |
| Stress on the conductor (MPa) | < 290 | |
| Average gap between layers (mm) | < 65 | |

### *Fabrication of poloidal coils.*

The superconducting poloidal coils are made of cable-in-conduit forced-flow conductor (CICC). Fabrication of two pairs of poloidal coils, the inner vertical field (IV) coils and the inner shaping (IS) field coils has been completed.

The largest poloidal coils, the outer vertical (OV) coils, are being constructed in the LHD experimental hall. The coil is composed of eight double pancakes with a nominal current of 30 kA. The major radius of the coil is 5.5 m, and its thickness is 0.54 m. The specifications of the coils are listed in Tables 3 and 4.

**Table 3.** Specifications of the poloidal coils

| | IV | IS | OV |
|---|---|---|---|
| Cooling type | Forced-flow | ← | ← |
| Inner/outer radii (m) | 1.6/2.1 | 2.7/3.1 | 5.4/5.8 |
| Height (m) | 0.46 | 0.46 | 0.54 |
| Number of pancakes | 16 | 16 | 16 |
| Number of turns | 15×16 = 240 | 13×16 = 208 | 9×16 = 144 |
| Operating current (kA) | 20.8 | 21.6 | 31.3 |
| Maximum field (T) | 6.5 | 5.4 | 5 |
| Stored energy (MJ) | 68 | 104 | 251 |
| Conductor length (km) | 2.7 | 3.7 | 5 |
| Number of flow paths | 16 | 16 | 16 |
| Length of flow paths (m) | 170 | 230 | 314 |

**Table 4.** Specifications of the poloidal conductors

| | IV | IS | OV |
|---|---|---|---|
| Type | Cable-in-conduit | ← | ← |
| Superconducting material | NbTi | ← | ← |
| Operating current (kA) | 20.8 | 21.6 | 31.3 |
| Critical current (kA) | 62.4 at 6.5 T | 64.8 at 5.4 T | 93.9 at 5.0 T |
| Conduit dimension (mm) | 23.0x27.6 | 23.0x27.6 | 27.5x31.8 |
| Thickness (mm) | 3 | 3 | 3.5 |
| Void fraction (%) | 38 | ← | ← |
| Strand diameter (mm) | 0.76 | 0.76 | 0.89 |
| Number of strands | 3x3x3x3x 6 = 486 | ← | ← |
| NbTi:Cu | 1:2.7 | 1:3.4 | 1:4.2 |
| Filament diameter (mm) | 15 | 12 | 14 |
| Strand surface | Bare | ← | ← |
| Inlet SHe pressure (Mpa) | 1.0–0.8 | ← | ← |
| Inlet SHe temperature (°K) | 4.5 | ← | ← |
| Flow rate per path (g/s) | 5 | 4.1 | 5 |
| Pressure drop per path (Mpa) | 0.1 | ← | ← |

### *Experiment of a single IV coil (EXSIV)*

The initial cooldown of the IV-L coil has been carried out. It took about 250 h to cool the coil from room temperature to 4.4°K. To prevent thermal stresses within the coil, the coil was cooled with less than 50°K temperature gradient between the inlet and the outlet. Fundamental tests for checking the electrical insulation and the joint between the conductors were performed with energizing the coil at 2.2 kA. The final test, which energizes the IV-L coil with 20.8 kA current, will be conducted within this year.

## Activity of the Plasma Heating Division

### *The development of high-current negative ion beam*

A 1/3 model of the real LHD ion source was used to extract 16.3 A of current at a current density of 30 mA/cm$^2$. The working gas pressure was reduced to 0.5 Pa. The extracted negative ion beam was accelerated to 125 keV. This beam current density already satisfies the specification required for the LHD neutral beam injector. Based on the success of the beam acceleration and physical study of the beam penetration, the design value of the beam energy was raised to 180 keV for hydrogen.

### Test of the ICRF power source

The test of the ICRF power source is progressing rapidly after improvements were made on the dummy load and on the cooling of the cavity of the final amplifier. Long pulse operations, 1.5 MW for 1 h and 1.9 MW for 10 s, have been conducted successfully. The former is regarded as a steady-state operation. Because the power source consists of two such tetrodes, this result suggests a capability of 3-MW ICRF power injection in steady state. R&D of a water cooled-antenna and transmission line is underway.

*ECH gyrotron and transmission line development*

An 84-GHz gyrotron (NIFS/Varian) was tested successfully on the test bench at the Toki site with the following records: 400 kW for 10 s and 500 kW for 2.2 s. Reflection from the dummy load was reduced carefully prior to the high power test. This is essential for development of steady state gyrotrons.

Development of a transmission system including a quasi-optical launcher has been almost finished: (a) sufficiently low transmission loss of the corrugated wave guide was demonstrated by the use of a 62-m long test wave guide; (b) a systematic method to design a 3-D quasi-optical transmission system was established; and (c) various aspects have been tested in CHS.

The development of high-power microwave windows needs to be continued.

Osamu Motojima, Director of Research Operations Division
National Institute for Fusion Science
322-6 Oroshicho, Toki 509-52, Japan
Phone: 81-572-57-5601
Fax: 582-57-5600
Furocho, Chikusaku, Nagoya 464-01, Japan
Phone: 81-52-789-4534
Fax: 52-789-4248
E-mail motojima@nifs.ac.jp